IOP Conference Series: Materials Science and Engineering

PAPER • **OPEN ACCESS**

Determination of the Thermal Stress Produced by a Thermo-poro-inclusion of Spheroid-shaped Near a Free Surface

To cite this article: X Zhang *et al* 2019 *IOP Conf. Ser.: Mater. Sci. Eng.* **576** 012043

View the article online for updates and enhancements.

This content was downloaded from IP address 107.150.122.145 on 15/10/2019 at 22:05

IOP Conf. Series: Materials Science and Engineering **576** (2019) 012043 doi:10.1088/1757-899X/576/1/012043

Determination of the Thermal Stress Produced by a Thermo-poro-inclusion of Spheroid-shaped Near a Free Surface

X Zhang[1], X Jin[1,2], P Li[1], D Lyu[1], and R Zhang[1]

[1]State Key Laboratory of Mechanical Transmissions, Chongqing University, Chongqing 400030, China
[2]College of Aerospace Engineering, Chongqing University, Chongqing, 400030, China

Corresponding Author's Email: jinxq@cqu.edu.cn

Abstract. Eshelby's inclusion with thermo-porous eigenstrain is a classical micromechanics problem, and may find wide applications in various engineering fields including mechanical transmission system, composite materials and geophysical structures. In this paper, the elastic field produced by thermo-porous spheroidal inclusion placed vertically near a free boundary surface is investigated. The current work complements our previous publication on the horizontally aligned spheroidal inclusion [Computers & Geosciences. 2019;122:15-24], and hence concludes that a complete elasticity solution with respect to the displacement, strain and stress can be obtained in closed-form. The elastic field of spheroidal inclusion due to thermal expansion is provided, and comparative study of inclusion due to fluid withdrawal leading to a decrease in pore pressure is discussed. The present half-space inclusion model can be used to determine the elastic fields of porous materials caused by produced by pore pressure fluctuation and temperature alteration.

1. Introduction

The Eshelby inclusion problem [1, 2] has broad applications in modern science and technology, as exemplified by the materials science and geophysical engineering [3]. However, a majority of the studies concern the inclusion in a full-space, whereas those on half-space problems are less reported in existing literatures due to mathematical complexity. Mindlin and Cheng [4] solved the spherical inclusion with uniform dilatational thermal expansion by utilizing the Galerkin vector stress function. Chiu [5] formulated the closed-form solution of uniformly distributed cuboidal inclusion by employing the method of images. Seo and Mura [6] studied the elastic stress field produced by a uniform thermal ellipsoidal inclusion in a semi-infinite space. The exterior solution of the inclusion problem is usually more intricate. Healy [7] and Manoylov et al. [8] respectively employed the spheroid-shaped inclusion model to solve the strain and stress fields of a penny-shaped crack, and the elastic properties of the porous material. Jin et al. [9] derived the displacement, deformation gradient, strain and stress Eshelby tensors and presented in a simpler and geometrically meaningful form. Lyu et al. [10] proposed analytical solutions for the complete elastic fields with respect to the displacements, strains, and stresses, produced by an ellipsoidal thermal inclusion in a half-space.

Due to the involved derivatives of elliptic integrals of the first and second kinds as well as tremendous mathematical difficulties arisen from the effect of the free boundary surface, the existing

Content from this work may be used under the terms of the Creative Commons Attribution 3.0 licence. Any further distribution of this work must maintain attribution to the author(s) and the title of the work, journal citation and DOI.
Published under licence by IOP Publishing Ltd

analytical solutions to half-space inclusion problems are usually lengthier and hence difficult for engineering applications. In a companion paper [11], the closed-form solution for horizontally aligned spheroidal inclusion subjected to the thermo-porous eigenstrain near free surface is obtained. Following this line of work, we present a complete elasticity solution corresponding to the displacement, strain and stress for the vertical alignment case. The current solution complements our previous publication on the horizontally placed spheroidal inclusion with thermo-porous eigenstrain [11] and concludes that a complete elasticity solution can be analytically presented in closed-form. In addition, several illustrating examples are provided to validate the present solution.

2. Formulation

2.1. Thermo-porous eigenstrain

Eigenstrain is the stress-free transform strain which encompasses a wide range of nonelastic strains including plastic strain, misfit strain and lattice mismatch, etc. As typical applications in geophysical engineering, the thermoelastic and poroelastic eigenstrains are employed to characterize the temperature change and pore pressure fluctuation, respectively. For an isotropic thermo-poroelastic medium, the eigenstrain, ε_{ij}^{*}, of poroelastic and thermoelastic couplings may be written as [11]

$$\varepsilon_{ij}^{*}=\frac{1-2\nu}{2\mu\left(1+\nu\right)}\delta_{ij}\alpha_{B}\Delta P+\delta_{ij}\lambda_{T}\Delta T \tag{1}$$

where the change of pore pressure and temperature are denoted by ΔP and ΔT, and μ, ν are the shear modulus and Poisson's ratio. Kronecker's delta, δ_{ij}, is defined as 1 if $i=j$ and 0 if $i\neq j$. Moreover, Boit pore-pressure coefficient is denoted by α_{B}, and coefficient of thermal expansion, λ_{T}, is used to describe the tendency of matter to change in shape, area, and volume in response to a change in temperature.

2.2. Thermo-porous ellipsoidal inclusion in a half-space

Consider a semi-infinite matrix (Figure. 1) containing a thermo-porous ellipsoidal inclusion, Ω, which is bounded by

$$\frac{x_1^2}{a_1^2}+\frac{x_2^2}{a_2^2}+\frac{\left(x_3-c\right)^2}{a_3^2}\leq 1 \qquad \left(c\geq x_3\right) \tag{2}$$

where $a_I\left(I=1,2,3\right)$ is the semi-axis of the ellipsoidal inclusion, *c* represents the depth of the inclusion. It is noted that the boundary surface $\left(x_3=0\right)$ is free from any external force. The uniform thermo-porous eigenstrain (Eq. (1)), is prescribed in Ω and vanished in the remainder of the matrix. (i.e. $\varepsilon_{11}^{*}=\varepsilon_{22}^{*}=\varepsilon_{33}^{*}=\varepsilon^{*}$ and $\varepsilon_{12}^{*}=\varepsilon_{13}^{*}=\varepsilon_{23}^{*}=0$).

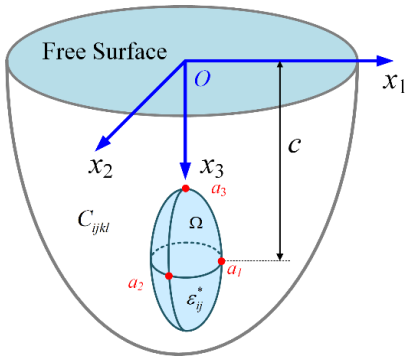

Figure 1. An ellipsoidal inclusion in a half-space.

The exterior displacement solution of the thermo-porous ellipsoidal inclusion in a semi-infinite space may be analytically presented as

$$u_i(\mathbf{x}) = \frac{(1+\nu)\varepsilon^*}{1-\nu}\begin{Bmatrix} x_i \mathcal{J}_I(\lambda) - 2x_3\left[\rho^*_{123} n^*_3 n^*_i - \delta_{3i}\mathcal{J}_I(\lambda^*)\right] \\ +(3-4\nu)\left[x_i \mathcal{J}_I(\lambda^*) - 2\delta_{3i} x_I \mathcal{J}_I(\lambda^*)\right] \end{Bmatrix} \tag{3}$$

for *i*=1, 2

$$u_i(\mathbf{x}) = \frac{(1+\nu)\varepsilon^*}{1-\nu}\begin{Bmatrix} (x_i - c)\mathcal{J}_I(\lambda) - 2x_3\left[\rho^*_{123} n^*_3 n^*_i - \delta_{3i}\mathcal{J}_I(\lambda^*)\right] \\ +(3-4\nu)\begin{bmatrix}(x_i + c)\mathcal{J}_I(\lambda^*) \\ -2\delta_{3i}(x_I + c)\mathcal{J}_I(\lambda^*)\end{bmatrix} \end{Bmatrix} \tag{4}$$

for *i*=3, and λ, λ^* are the maximum positive root of cubic equations with respect to the imaginary and imaginary confocal ellipsoids. The function $\mathcal{J}_I$, ρ^*_{123} and unit normal vectors n_i, n^*_i are omitted here due to length, and interested readers are referred to [10, 11].

The exterior strain solution may be expressed as

$$\varepsilon_{ij}(\mathbf{x}) = \frac{(1+\nu)\varepsilon^*}{1-\nu}\begin{Bmatrix} \underline{\underline{\delta_{ij}\mathcal{J}_I(\lambda) - \rho_{123} n_i n_j}} - \delta_{3I}\delta_{ij}(4-8\nu)\mathcal{J}_3(\lambda^*) \\ +(3-4\nu)\left[\delta_{ij}\mathcal{J}_I(\lambda^*) - \rho^*_{123} n^*_i n^*_j\right] \\ -4\nu\rho^*_{123}\left(\delta_{3i} n^*_I n^*_j + \delta_{3j} n^*_i n^*_J\right) \\ +2\rho^*_{123}\left[M_{ij}(\lambda^*) + N_{ij}(\lambda^*)\right] \end{Bmatrix} \tag{5}$$

for *i*=1, 2, 3, and terms M_{ij}, N_{ij} are

$$M_{ij}(\lambda^*) = \frac{x_3 n^*_3 n^*_i n^*_j}{\sqrt{H(\lambda^*)}}\left(\frac{1-4n^*_1 n^*_1}{a_1^2+\lambda^*} + \frac{1-4n^*_2 n^*_2}{a_2^2+\lambda^*} + \frac{1-4n^*_3 n^*_3}{a_3^2+\lambda^*} + \frac{2}{a_I^2+\lambda^*} + \frac{2}{a_J^2+\lambda^*} + \frac{2}{a_3^2+\lambda^*}\right) \tag{6}$$

$$N_{ij}(\lambda^*) = \frac{\left(\delta_{3i} n^*_j + \delta_{3j} n^*_i\right)c}{\sqrt{H(\lambda^*)}\left(a_3^2+\lambda^*\right)} - \frac{\delta_{ij} x_3 n^*_3}{\sqrt{H(\lambda^*)}\left(a_I^2+\lambda^*\right)} \tag{7}$$

According to Hooke's law, the exterior stress solution may also be determined in an explicit form

$$\sigma^{out}_{ij}(\mathbf{x}) = \frac{2\mu(1+\nu)\varepsilon^*}{1-\nu}\begin{Bmatrix} \delta_{ij}\mathcal{J}_I(\lambda) - \rho_{123} n_i n_j \\ \underline{\underline{-(4-8\nu)\delta_{3I}\delta_{ij}\mathcal{J}_I(\lambda^*)}} \\ +(3-4\nu)\left[\delta_{ij}\mathcal{J}_I(\lambda^*) - \rho^*_{123} n^*_i n^*_j\right] \\ -4\nu\left(\delta_{3I} + \delta_{3J}\right)\rho^*_{123} n^*_i n^*_j \\ +4\nu\delta_{ij}\left[\rho^*_{123} n^*_3 n^*_3 - \mathcal{J}_3(\lambda^*)\right] \\ +2\rho^*_{123}\left[M_{ij}(\lambda^*) + N_{ij}(\lambda^*)\right] \end{Bmatrix} \tag{8}$$

2.3. In the case of spheroidal inclusion

By setting $a_1 = a_2 \neq a_3$ and $\alpha = a_3 / a_1$, λ for the spheroidal inclusion is thus derived explicitly as

$$\lambda=\frac{1}{2}\left\{\begin{array}{l}x_1^2+x_2^2+\left(x_3-c\right)^2-a_1^2-a_2^2+\\ \sqrt{\left[x_1^2+x_2^2+\left(x_3-c\right)^2+a_1^2-a_2^2\right]^2+4\left(a_2^2-a_1^2\right)x_1^2}\end{array}\right\} \tag{9}$$

and the corresponding $\mathcal{I}_3$ function is

$$\mathcal{I}_3\left(\lambda\right)=\frac{\alpha}{\left(1-\alpha^2\right)^{\frac{3}{2}}}\left(\tan\varpi-\varpi\right) \tag{10}$$

for oblate spheroid $\left(\alpha<1\right)$, and

$$\mathcal{I}_3\left(\lambda\right)=\frac{\alpha}{\left(\alpha^2-1\right)^{\frac{3}{2}}}\left[-\ln\left(\tan\frac{\omega}{2}\right)-\cos\omega\right] \tag{11}$$

for prolate spheroid $\left(\alpha>1\right)$. Moreover, quantities in Eqs. (10) and (11) are

$$\varpi=\arccos\sqrt{\frac{a_3^2+\lambda}{a_1^2+\lambda}},\quad \omega=\arcsin\sqrt{\frac{a_1^2+\lambda}{a_3^2+\lambda}} \tag{12}$$

The elastic field caused by a thermo-porous spheroidal ellipsoidal inclusion near free surface may be analytically obtained. The displacement solution for the exterior field is

$$u_1\left(\mathbf{x}\right)=\frac{\left(1+\nu\right)\varepsilon^*}{1-\nu}\left\{\begin{array}{l}\frac{x_1}{2}\left[\rho_{13}-\mathcal{I}_3\left(\lambda\right)\right]-2x_3\rho_{13}^*n_1^*n_3^*\\ +\left(\frac{3}{2}-2\nu\right)x_1\left[\rho_{13}^*-\mathcal{I}_3\left(\lambda^*\right)\right]\end{array}\right\} \tag{13}$$

$$u_2\left(\mathbf{x}\right)=\frac{\left(1+\nu\right)\varepsilon^*}{1-\nu}\left\{\begin{array}{l}\frac{x_2}{2}\left[\rho_{13}-\mathcal{I}_3\left(\lambda\right)\right]-2x_3\rho_{13}^*n_2^*n_3^*\\ +\left(\frac{3}{2}-2\nu\right)x_2\left[\rho_{13}^*-\mathcal{I}_3\left(\lambda^*\right)\right]\end{array}\right\} \tag{14}$$

$$u_3\left(\mathbf{x}\right)=\frac{\left(1+\nu\right)\varepsilon^*}{1-\nu}\left\{\begin{array}{l}\left(x_3-c\right)\mathcal{I}_3\left(\lambda\right)-2x_3\rho_{13}^*n_3^*n_3^*\\ +\left[2x_3+\left(4\nu-3\right)\left(x_3+c\right)\right]\mathcal{I}_3\left(\lambda^*\right)\end{array}\right\} \tag{15}$$

The corresponding exterior strain and stress solutions can be derived in closed-form through Eqs. (5)and (8). The detail formulation is omitted here due to length.

3. Results and discussions

The stress field of a thermal spheroidal inclusion in a half-space was reported by Seo and Mura [6]. In this section, the elastic fields corresponding to the displacement, strain and stress for the thermo-porous inclusion near free surface is carried out with $E=210\text{GPa}$ and $\nu=0.3$. The stress distributions for the spheroidal inclusion with thermal eigenstrain may serve as a benchmark example to validate the present solution.

For the spheroidal inclusion ($3a_1=3a_2=a_3$) centered at ($0,\ 0,\ a_3$) subjected to thermal eigenstrain, the displacements along the x_1-direction are plotted in Figure. 2. The displacement components are normalized by $u_0=\lambda_T\Delta Ta_1$. It can be seen from Figure. 2 that the displacements are continuous across

the interface between the inclusion and surrounding matrix. The displacement u_1 represents tension both inside and outside the inclusion, while u_3 shows compression.

The strain distributions along the x_1-direction are illustrated in Figure. 3. The strain components are normalized by $\varepsilon_0 = \lambda_T \Delta T$, and the strains in the interior field are no longer constant due to the existence of the free surface, as opposed to the case of full-space [9].

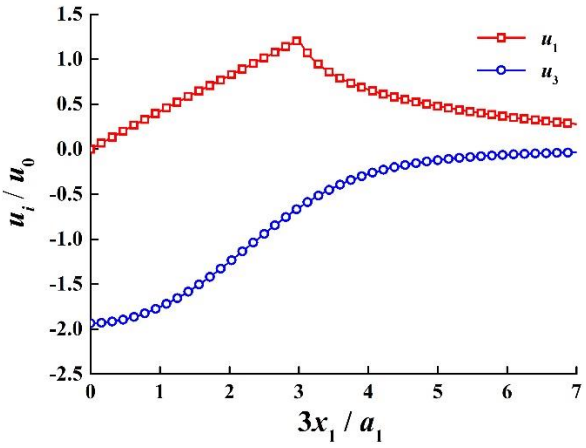

Figure 2. Displacements of a thermal spheroidal inclusion

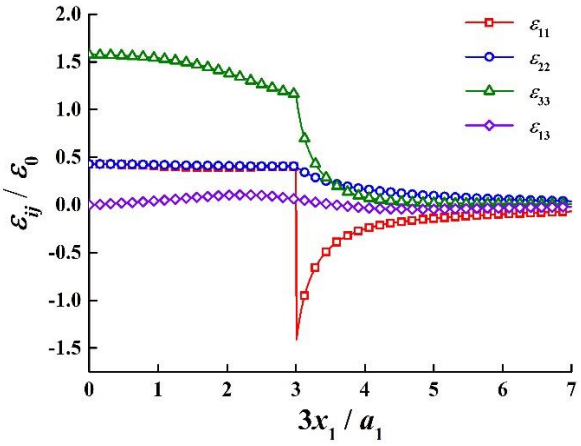

Figure 3. Strains of a thermal spheroidal inclusion

The stresses are normalized by $\sigma_0 = E\lambda_T \Delta T / (1-\nu)$, and the variations along the x_1-direction are shown in Figure. 4. The normal stress components σ_{22} and σ_{33} suffer discontinuities across the interface, and become almost zero for $x_1 / a_3 > 7$.

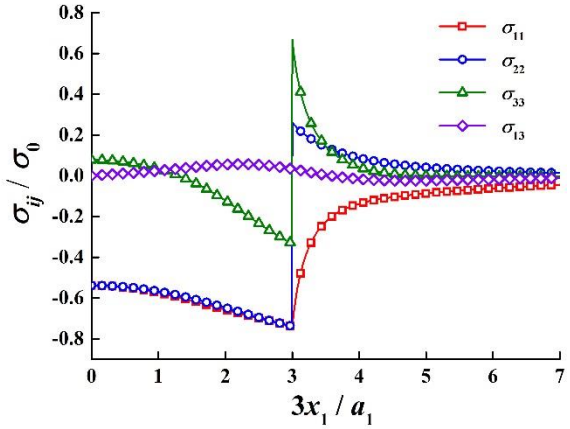

Figure 4. Stresses of a thermal spheroidal inclusion

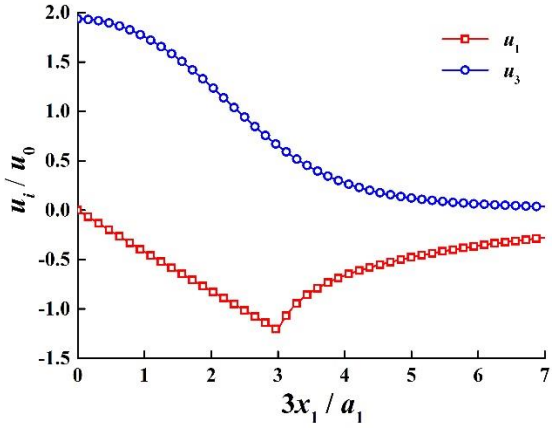

Figure 5. Displacements of a spheroidal inclusion subjected to the porous eigenstrain in a half-space

The results of the elastic field for the spheroidal inclusion subjected to the porous eigenstrain are studied, where the size of porous inclusion and depth location are identical to the case of thermal inclusion. In this work, all the displacement, strain and stress components are normalized respectively by $u_0 = -(1-2\nu)\alpha_B \Delta P / E a_1$, $\varepsilon_0 = -(1-2\nu)\alpha_B \Delta P / E$ and $\sigma_0 = -\alpha_B \Delta P$. The corresponding elasticity

solution with respect to the displacements, strains and stresses along the x_1 -direction are illustrated in Figures. 5-7 in sequence. It is noted that the prescribed thermal eigenstrain is caused by temperature change resulting in a localized heating, while the porous eigenstrain is produced by fluid migration leading to a decrease in pore pressure.

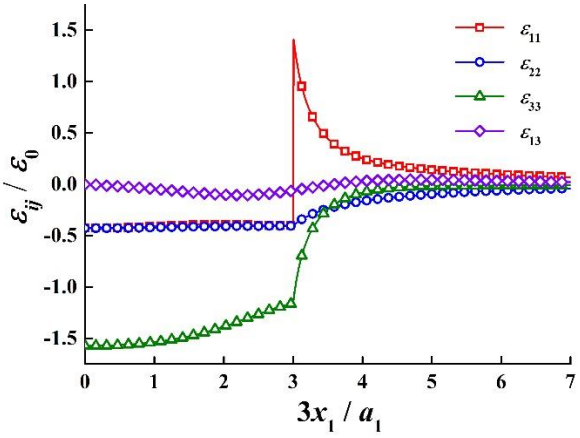

Figure 6. Strains of a spheroidal inclusion with porous eigenstrain near the surface

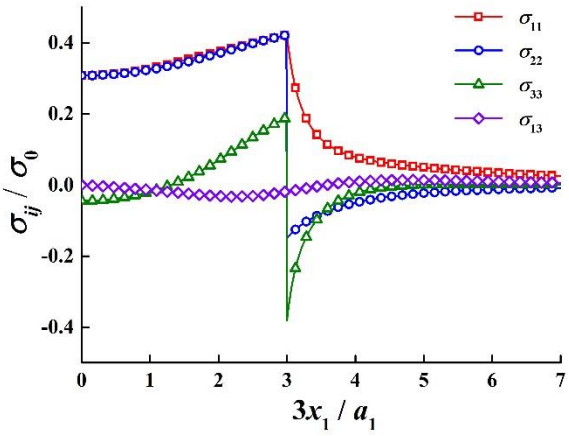

Figure 7. Stresses of a porous spheroidal inclusion in a semi-infinitely extended matrix

4. Concluding remarks

The current work investigates the solution of the complete elastic field for a spheroidal inclusion with thermo-porous eigenstrain vertically placed in a half-space. This complements our previous publication [11] on the horizontally aligned thermo-porous spheroidal inclusion in a half-space. The elastic fields for both the prolate and oblate spheroidal inclusions are derived based on the degenerate case of ellipsoidal inclusion near free surface. The present formulation of the displacements, strains and stresses are presented in closed-form, for convenience of engineering applications.

Jump conditions are discussed to interpret that the discontinuities are only depending on the terms without superscript "*". The effects of geometry for both oblate and prolate spheroidal inclusions are examined in response to the alteration of eigenstrains which include the thermal eigenstrain due to localized heating and porous eigenstran caused by fluid withdrawal leading to a decrease in pore pressure. It is demonstrated that the proposed inclusion model can be employed to predict the elastic fields of porous materials produced by thermal and porous eigenstains near a free surface.

5. References

[1] J. Eshelby, P Roy Soc A-Math Phy, **241**(1226), 376-396 (1957)
[2] J. Eshelby, P Roy Soc A-Math Phy, **252**(1271), 561-569 (1959)
[3] K. Zhou, H. Hoh, X. Wang, L. Keer, J. Pang, B. Song, Q. Wang, Mech Mater, **60**, 144-158 (2013)
[4] R. Mindlin, D. Cheng, J Appl Phys, **21**(9), 931-933 (1950)
[5] Y. Chiu, J Appl Mech-T ASME, **45**(2), 302-306 (1978)
[6] K. Seo, T. Mura, J Appl Mech-T ASME, **46**(3), 568-572 (1979)
[7] D. Healy, Comput Geosci, **35**(10), 2170-2173 (2009)
[8] A. Manoylov, F. Borodich, H. Evans, P Roy Soc A-Math Phy, **469**(2154), 20120689 (2013)
[9] X. Jin, D. Lyu, X. Zhang, Q. Zhou, Q. Wang, L. Keer, J Appl Mech-T ASME, **83**(12), 121010-12 (2016)
[10] D. Lyu, X. Zhang, P. Li, D. Luo, Y. Hu, X. Jin, L. Zhang, L. Keer, J Appl Mech-T ASME, **85**(5), 051005-8 (2018)
[11] X. Zhang, D. Lyu, P. Li, X. Jin, P. Liaw, L. Keer, Comput Geosci, **122**, 15-24 (2019)

Acknowledgments
This work is supported by Fundamental Research Funds for the Central Universities (2018CDYJSY0055 and 106112017CDJQJ328839), and the Graduate Research and Innovation Foundation of Chongqing, China (Nos. CYB17025 and CYB18020). X.J. would like to acknowledge the support from the National Natural Science Foundation of China (Nos. 51475057 and 51875059), and the State Key Laboratory of Mechanical Transmissions (SKLMT-ZZKT-2017M15).